



Transport induced patterns in an optical system with focussing nonlinearity

P.L. Ramazza, S. Boccaletti, F.T. Arecchi

Istituto Nazionale di Ottica, I-50125 Florence, Italy

Received 14 August 1996; accepted 29 October 1996

Abstract

We report the experimental sequence of pattern forming instabilities that a nonlocal interaction, due to a lateral image transport in the feedback loop, induces in an optical system with focussing nonlinearity. As the lateral transport is increased, the transitions between consecutive patterns differ both qualitatively and quantitatively from those already observed in a system with defocussing nonlinearity. In particular, we show evidence of a new bifurcation leading to the appearance of nonequilateral hexagons, which become equilateral for a particular nonzero value of the lateral transport.

PACS: 42.65.-k; 03.40.Kf; 42.60.Jf; 89.90.+n

1. Introduction

Pattern forming instabilities occurring in systems formed by an optically nonlinear component inserted in a feedback loop are presently a subject of wide experimental and theoretical investigation [1–8]. Nonlinear components commonly used in these systems are either slices of some optically nonlinear medium, or composite devices based on liquid crystals (liquid crystal light valves).

The formation of structures in systems of this kind results from the combination of two basic mechanisms. First, perturbations of the optical intensity are converted to perturbations of the optical phase by means of the nonlinear component (Kerr-like nonlinearity); second, perturbations of the optical phase are converted to perturbation of the optical intensity via diffraction (or via interference) in the feedback loop. This process results in the destabilization of certain preferred wavevector bands.

In the present paper we investigate the influence of nonlocal interactions, introduced in the system via a wavefront translation Δx in the feedback loop, on the pattern forming instabilities in a system of this kind. The introduction of a long range interaction in these systems is not novel per se. Effects of a nonlocality obtained via a rotation of the wavefront have been dealt with both experi-

mentally [5,9,10] and theoretically [11,12]. Situations in which a lateral transport is present have also been reported for various experimental conditions. The nonlinear component used in these last experiments were either liquid crystals [13], or alkali vapours [14], or a liquid crystal light valve (LCLV) [15,16].

In the first two cases the range of the experimentally accessible values of the system Fresnel number $F = d^2/\lambda L$ (d is the illuminated diameter, L is the free propagation length in the feedback loop) is strongly limited. This fact is due to the relatively small nonlinear optical coefficients of the media used, that obliges to concentrate a strong laser beam on a small area. The problem is overcome by use of a LCLV as a nonlinear device. Notice that since each elementary spot has a size $a \sim \sqrt{\lambda L}$, F corresponds to the square of what is in general called the geometric aspect ratio d/a . A large F means a large number of periodic spots and hence a reduced influence of the boundary perturbations [17].

Experiments performed using a LCLV [16] have shown the existence of a series of transitions between different patterns, for increasing Δx . The scenario is similar to the one observable in hydrodynamical convection when increasing a pump parameter, with the sequential occurrence of hexagons, rolls, cross-rolls and zig-zag patterns. The

experiment of Ref. [16] was limited to the case in which the nonlinearity of the system is of defocussing type. Here we present the results obtained in similar conditions, but using a focussing nonlinearity.

The change in the sign of the nonlinearity has relevant consequences on the observed instabilities, both from a qualitative and a quantitative point of view. In particular, the focussing case presents for $\Delta x \neq 0$ a series of states patterned with nonequilateral hexagons, that do not exist in the defocussing case. Another difference is the fact that in the present case all the instabilities involve only one wavenumber band in the Fourier space, instead of the two involved in the defocussing case. These features of the observed scenario are simply explained by a linear stability analysis of the problem.

2. Nonlocality induced pattern selection

The experimental setup, shown in Fig. 1, consists of a liquid crystal light valve (LCLV) with diffractive feedback [5]. A lateral displacement Δx of the wavefront in the feedback loop introduces nonlocal interaction of the signal with itself. The relevant dynamical variables of the system are the extraordinary component $n(\mathbf{r}, t)$ of the LCLV index of refraction and the optical field $E(\mathbf{r}, z, t)$. We denote with $\mathbf{r} \equiv (x, y)$ the coordinates of a plane transverse to the light propagation, and with z the propagation axis. Coupling of n and E due to optical nonlinearity and diffraction results in a unique equation for n describing the evolution of the system [2]:

$$\tau \frac{\partial n(x, y, t)}{\partial t} = -n(x, y, t) + I_d^2 \nabla_{\perp}^2 n(x, y, t) + \alpha T_x \{ I_0 \exp[i(L/2k_0) \nabla_{\perp}^2] \exp[i n(x, y, t)] \}^2. \quad (1)$$

Here, $\tau = 100$ ms, $I_d = 40 \mu\text{m}$ are respectively the response time and the diffusion length of the LCLV, ∇_{\perp}^2 is the Laplacian operator in the (x, y) plane,

$$I_0 \exp[i(L/2k_0) \nabla_{\perp}^2] \exp[i n(x, y, t)]^2$$

is the intensity distribution resulting from the free propagation along a distance L of the phase modulated field $E_0 \exp[i n(x, y)]$, $I_0 = |E_0|^2$ is the input intensity, and T_x is a translation operator such as $T_x[I_0(x, y)] \equiv I_0(x + \Delta x, y)$. The coefficient α gives the strength and the sign of the Kerr nonlinearity ($\alpha > 0$ for focussing media, $\alpha < 0$ for defocussing media).

In the case of the LCLV, the feedback coefficient α is negative [18].

In the present problem, however, a change in the sign of the propagation distance L is fully equivalent to a change in the sign of the nonlinearity for all the Fourier

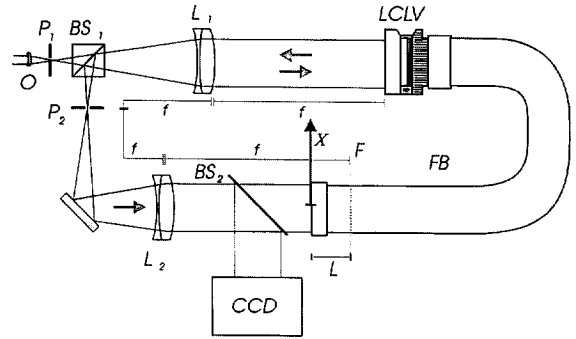


Fig. 1. Experimental setup. O – microscope objective; P_1, P_2 – pinholes; BS_1, BS_2 – beam splitters; LCLV – liquid crystal light valve; L_1, L_2 – lenses of $f = 25$ cm focal length; FB – fiber bundle; CCD – videocamera; L – free propagation length; X – direction of transport. The $4f$ configuration of the feedback loop provides a 1 to 1 imaging of the front plane of the LCLV on the F plane.

components of n except the continuous one [6]. Change of the sign of L is easily obtained in the experiment via a proper choice of lenses inserted in the feedback loop [19]. In these conditions, the nonlinearity of the overall system (LCLV + propagation) is of focussing type.

For all the measurements here reported, we kept fixed the amplitude and frequency of the voltage applied to the LCLV at $V_0 = 10$ V rms and $\nu = 1.5$ kHz respectively, and the propagation distance $L = 38$ cm (in the following we will indicate by L the modulus of the propagation length, which is actually negative). The input intensity is provided by an Ar^+ laser operating at $\lambda = 514$ nm.

In a first set of observations we set the input intensity at $I_0 = 23 \mu\text{W}/\text{cm}^2$, and gradually increase the value of Δx . The intensity patterns observed in these conditions are reported in Fig. 2 together with the far field patterns corresponding to the Fourier spectra.

For Δx close to 0, a hexagonal pattern is observed. The hexagons here are not oriented along some privileged direction, across the whole wavefront. Rather, domains with hexagons oriented along all the possible directions fill the plane, as evidenced by the fact that the Fourier spectrum (Fig. 2a') is not made by a single hexagonal set of spots, but by many hexagonal sets angularly separated and filling almost uniformly a ring of constant radius.

In the range $70 \mu\text{m} < \Delta x < 510 \mu\text{m}$, a horizontal roll pattern is dominating. This structure is replaced by a square pattern for a range of Δx between $520 \mu\text{m}$ and $560 \mu\text{m}$. A further increase of Δx results in the appearance of a very regular tiling of the plane with hexagons ($600 \mu\text{m} < \Delta x < 770 \mu\text{m}$). At variance with the hexagons observed for $\Delta x = 0$, these ones are oriented along a preferred direction, as shown by the defined spots in the Fourier space. The absence of defects in the texture is nearly total.

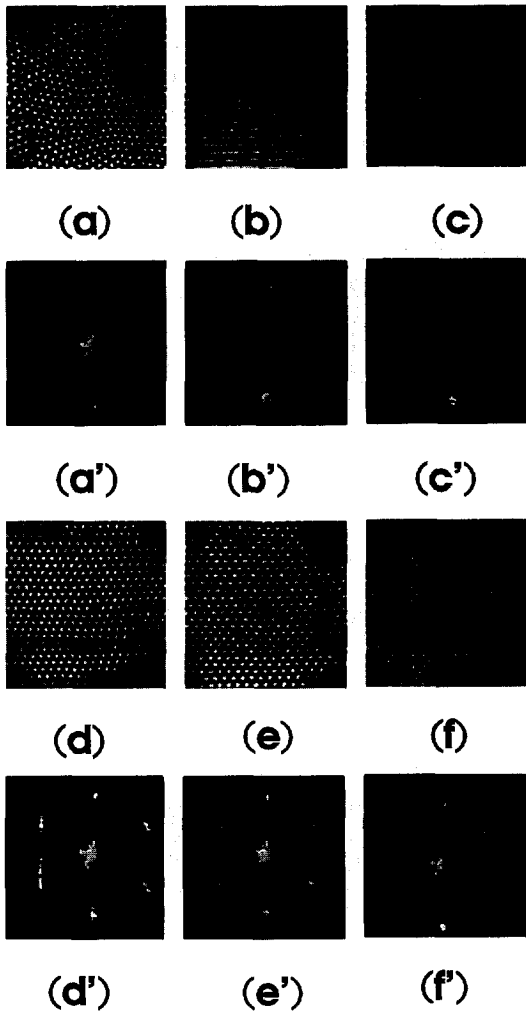


Fig. 2. Experimental near field (a–f) and far field (a'–f') patterns observed at $I_0 = 23 \mu\text{W}/\text{cm}^2$ for different Δx . (a, a') $\Delta x = 0 \mu\text{m}$, hexagons; (b, b') $\Delta x = 290 \mu\text{m}$, horizontal rolls; (c, c') $\Delta x = 520 \mu\text{m}$, cross rolls; (d, d') $\Delta x = 640 \mu\text{m}$, hexagons; (e, e') $\Delta x = 740 \mu\text{m}$, hexagons; (f, f') $\Delta x = 840 \mu\text{m}$, domain pattern. The free propagation length is $L = 38 \text{ cm}$.

In general, these hexagons are nonequilateral, the ratio between their sides depending on the values of Δx . Nonequilateral hexagons have been observed previously in chemical reactions [20] and in Rayleigh-Bénard convection [21]. A theoretical approach [22] has predicted the existence and studied the stability of these structures for the case in which the rotational symmetry of the system is broken, as it is our case. However, the analysis of Ref. [22] relies on the coupling of three modal amplitudes via purely real coefficients. On the contrary, the introduction of the displacement in the feedback loop implies complex coefficients in the modal equations as referred to our problem, therefore a direct application of the predictions of Ref. [22] to our case would not be appropriate.

For very large values of Δx ($\Delta x > 780 \mu\text{m}$), the hexagonal pattern breaks into domains (Fig. 2f, f') each one filled by a different combination of excited modes.

Information on the observed scenario can be gained by linear stability analysis (LSA). Temporal and spatial Fourier transformation of Eq. (1) provides relations for the real and imaginary part of the eigenvalue $\lambda_q + i\omega_q$ associated with the perturbations at wavevector q :

$$\tau\lambda_q = -1 - I_d^2 q^2 + 2\alpha I_0 \sin\left(\frac{q^2 L}{2k_0}\right) \cos(q\Delta x \cos\phi), \tag{2a}$$

$$\tau\omega_q = 2\alpha I_0 \sin\left(\frac{q^2 L}{2k_0}\right) \sin(q\Delta x \cos\phi), \tag{2b}$$

where $k_0 \equiv 2\pi/\lambda$ is the optical wavenumber, q is the modulus of q , and ϕ is the angle between q and Δx . The diffractive term $\sin(q^2 L/2k_0)$ accounts for the free propagation within the optical feedback loop.

The fundamental set of modes that maximizes the real part of the eigenvalue are expected to first destabilize at threshold. They are:

$$\phi = \pm \frac{\pi}{2}, \quad q \approx \sqrt{\frac{\pi k_0}{L}} \quad (\text{horizontal rolls}), \tag{3a}$$

$$\phi = 0, \pi, \quad q = q(\Delta x) \quad (\text{vertical rolls}), \tag{3b}$$

$$\phi = \pm \arccos\left(\frac{2\pi}{q\Delta x}\right), \quad q \approx \sqrt{\frac{\pi k_0}{L}} \quad (\text{oblique rolls}). \tag{3c}$$

With respect to the analogous expression for the defocussing case [16], we notice two main differences. First, the oblique roll solution exists now for $|q\Delta x/2\pi| < 1$, instead of $|q\Delta x/\pi| < 1$. Second, both the horizontal and the oblique roll modes lie in this case on the band $q \approx \sqrt{\pi k_0/L}$. This fact leads to the consequence that the horizontal and the oblique roll modes have the same threshold intensity I_{th} . The threshold of the vertical roll mode is larger than I_{th} except for a single value of Δx ($\Delta x = 520 \mu\text{m}$).

Since the eigenvalue associated to the vertical roll mode has a nonzero imaginary part, the square pattern observed around $\Delta x = 520 \mu\text{m}$ is drifting with a velocity of the order of $100 \mu\text{m}/\text{s}$. All the other patterns observed are stationary in time, since they arise from bifurcations of modes having zero imaginary part. This is at variance with the situation occurring in one-dimensional systems [14,15], in which drifting patterns are generic.

Fig. 3 presents the theoretical threshold curves for the three solutions considered, together with the experimental values of the measured threshold intensities. The bifurcation of the hexagons at $\Delta x = 0$ is subcritical, and it

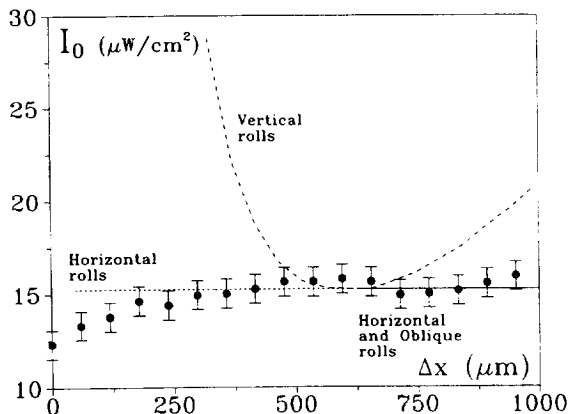


Fig. 3. Experimental and theoretical thresholds for pattern formation. The long (short) dashed line is the threshold calculated for vertical (horizontal) rolls, the solid line is the theoretical threshold for both horizontal and oblique rolls. The full circles represent the experimental measurements with the corresponding error bars. The Kerr coefficient used in the calculation is $\alpha = 0.072 \text{ cm}^2 / \mu\text{W}$.

requires considering nonlinear cooperative terms between modes [23]. This explains the discrepancy between the measured thresholds and the ones predicted by LSA. For all the other observed patterns, the agreement between theory and experiment is good.

3. Intensity controlled bifurcations

In this section we report the results of a series of observations performed by keeping fixed the value of Δx and increasing the input intensity I_0 from below to above the threshold of pattern formation. We find it useful to introduce the above-threshold parameter $\epsilon \equiv (I_0 - I_{0,\text{th}}) / I_{0,\text{th}}$.

For $\Delta x < 500 \mu\text{m}$ and for $\Delta x > 820 \mu\text{m}$, the patterns observed close to threshold do not change qualitatively when ϵ is increased up to a value of the order of unity. An example is shown in Fig. 4. In this case, the domain structure of the wavefront is present for any value of ϵ .

At the intermediate values of Δx for which hexagons are observed, a different behavior appears. As an example, we show in Fig. 5 that, for $\Delta x = 600 \mu\text{m}$, a pattern formed by vertical rolls and squares is first destabilized for $\epsilon \approx 0.2$. This is in agreement with the results of LSA (see Fig. 3). Increasing ϵ up to 0.55, vertical rolls are nearly suppressed, and hexagons begin to appear together with the previously existing squares. Finally, for $\epsilon = 1$, the hexagonal pattern is the dominating one, though some remnants of squares still exist.

This fact suggests that the formation of hexagons is due to a secondary bifurcation. We notice that the observed hexagons are due to a superposition of the horizontal roll

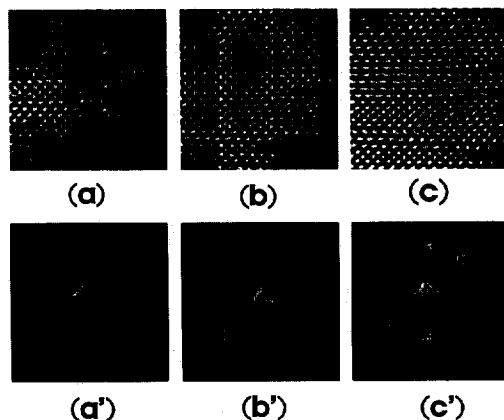


Fig. 4. Experimental near field (a–c) and far field (a'–c') patterns observed at $\Delta x = 840 \mu\text{m}$ for different values of the input intensity. (a, a') $I_0 = 18 \mu\text{W}/\text{cm}^2$ ($\epsilon = 0.2$, close to threshold); (b, b') $I_0 = 23 \mu\text{W}/\text{cm}^2$ ($\epsilon = 0.55$); (c, c') $I_0 = 30 \mu\text{W}/\text{cm}^2$ ($\epsilon = 1$).

and oblique roll modes predicted by LSA. The fact that the ratio between the sides of the hexagons depends on Δx follows from the dependence on Δx of the angle ϕ formed by the oblique rolls with the x axis. A necessary requirement for the existence of hexagonal tiling is that the sum of the three excited wavevectors be $\mathbf{q}_1 + \mathbf{q}_2 + \mathbf{q}_3 = 0$. This closure condition leads, in the presence of a quadratic nonlinearity, to mode–mode cooperation, resulting e.g. in the subcritical bifurcation of hexagons for $\Delta x = 0$ [23]. When $\Delta x \neq 0$, however, the closure condition is not necessarily satisfied for the triad of wavevectors allowed at threshold by LSA.

In Fig. 6 we plot as a function of Δx the quantity

$$\Delta q \equiv \frac{|q_1 + q_2 + q_3|}{|q_1| + |q_2| + |q_3|}, \quad (4)$$

where q_1, q_2, q_3 are the unstable modes predicted by LSA

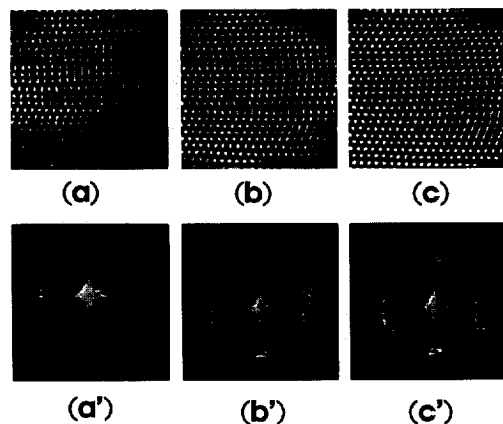


Fig. 5. Same as Fig. 3 with $\Delta x = 600 \mu\text{m}$. Hexagonal patterns are observed only far above threshold.

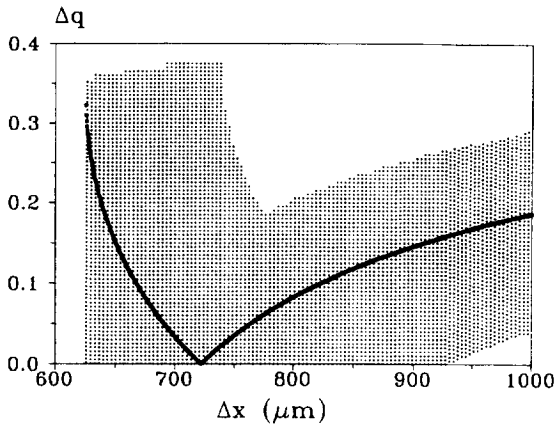


Fig. 6. Plot of the mismatch Δq (see text for definition) as a function of the transverse displacement Δx . The solid line represents the values of Δq calculated at threshold for each Δx . The shadowed region delimits the range of Δq spanned when the broadening for q_j , ($j=1, 2, 3$) is considered, for a value of the above-threshold parameter $\epsilon = 0.05$.

for $\Delta x \geq 620 \mu\text{m}$. Δq represents a normalized mismatch of the triad of vectors with respect to the closure condition. It can be seen that, at threshold, Δq vanishes only for a single value of Δx , close to $720 \mu\text{m}$. Hence, we expect that hexagon formation at threshold is possible only in the vicinity of this point. This is confirmed by the pattern observed at $\Delta x = 720 \mu\text{m}$, and reported in Fig. 7.

If Δx differs from this especial value, the triad of wavevectors is not resonant at threshold. However, when ϵ is increased, broadening of the unstable band results in a broadening of the range of Δx for which the closure condition $\Delta q = 0$ can be satisfied. Once ϵ has been fixed, for any triad (q_1, q_2, q_3) which is linearly unstable ($\lambda_{q_1} > 0$, $\lambda_{q_2} > 0$ and $\lambda_{q_3} > 0$), we have calculated the value of the mismatch Δq . The shadowed region of Fig. 6 reports the

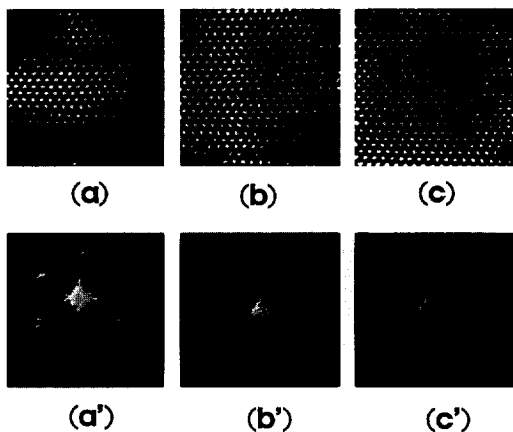


Fig. 7. Same as Fig. 3 with $\Delta x = 720 \mu\text{m}$. In this case, hexagons are present also at threshold.

results of this procedure for $\epsilon = 0.05$. The closure condition can be now fulfilled in the range $620 \mu\text{m} < \Delta x < 900 \mu\text{m}$.

This explains the fact that, except for a specific, small range of Δx , the transition to hexagons for increasing pump intensity is observed as a secondary bifurcation.

4. Conclusions

In summary, by introducing a negative propagation length, through a suitable lens system, we transform a standard LCLV system into a system with focussing type nonlinearity. When we add a lateral transport Δx of the image in the feedback loop, we observe a new class of phenomena quite different from those already reported for the same Δx values in a defocussing medium.

A linear stability analysis of the model equations provides a consistent explanation of all the observations.

References

- [1] S.A. Akhmanov, M.A. Vorontsov and V.Yu. Ivanov, JETP Lett. 47 (1988) 707.
- [2] W.J. Firth, J. Mod. Optics 37 (1990) 151; G. D'Alessandro and W.J. Firth, Phys. Rev. Lett. 66 (1991) 2597.
- [3] G. Grynberg, E. Le Bihan, P. Verkerk, P. Simoneau, J.R.R. Leite, D. Bloch, S. Le Boiteux and M. Ducloy, Optics Comm. 67 (1988) 363.
- [4] R. Macdonald and H.J. Eichler, Optics Comm. 89 (1992) 289.
- [5] E. Pampaloni, P.L. Ramazza, S. Residori and F.T. Arecchi, Europhys. Lett. 25 (1994) 587; S. Residori, P.L. Ramazza, E. Pampaloni, S. Boccaletti and F.T. Arecchi, Phys. Rev. Lett. 76 (1996) 1063.
- [6] R. Neubecker, G.L. Oppo and T. Tschudi, Phys. Rev. A 52 (1995) 791.
- [7] M.A. Vorontsov and A.Y. Karpov, Optics Lett. 20 (1995) 2466, and references therein.
- [8] A.J. Scroggie and W.J. Firth, Phys. Rev. A 53 (1996) 2752, and references therein.
- [9] S.A. Akhmanov, M.A. Vorontsov, V.Yu. Ivanov, A.V. Larichev and N.I. Zheleznykh, J. Opt. Soc. Am. B 9 (1992) 78; P.L. Ramazza, S. Residori, E. Pampaloni and A.V. Larichev, Phys. Rev. A 53 (1996) 400.
- [10] E. Pampaloni, P.L. Ramazza, S. Residori and F.T. Arecchi, Phys. Rev. Lett. 74 (1995) 258.
- [11] H. Adachiara and H. Faid, J. Opt. Soc. Am. B 10 (1993) 1242.
- [12] M. LeBerre, A.S. Patrascu, E. Ressayre, A. Tallet and N.I. Zheleznykh, Chaos Solitons Fractals 4 (1994) 1389.
- [13] R. Macdonald and H. Danlewski, Optics Lett. 20 (1995) 441.
- [14] A. Petrossian, L. Dambly and G. Grynberg, Europhys. Lett. 29 (1995) 209.
- [15] P.L. Ramazza, P. Bigazzi, E. Pampaloni, S. Residori and F.T. Arecchi, Phys. Rev. E 52 (1995) 5524.
- [16] P.L. Ramazza, S. Boccaletti, A. Giaquinta, E. Pampaloni, S. Soria and F.T. Arecchi, Phys. Rev. A, September 1996.

- [17] F.T. Arecchi, S. Boccaletti, P.L. Ramazza and S. Residori, *Phys. Rev. Lett.* 70 (1993) 2277.
- [18] M.A. Vorontsov, M.E. Kirakosyan and A.V. Larichev, *Sov. J. Quantum Electron.* 21 (1991) 105 [*Kvantovaya Elektron.* 18 (1991) 117].
- [19] E. Ciaramella, M. Tamburrini and E. Santamato, *Appl. Phys. Lett.* 69 (12) (1993) 1604.
- [20] Q. Ouyang and H. Swinney, *Nature* 352 (1991) 610.
- [21] G. Ahlers, L.J. Berge and D.S. Cannell, *Phys. Rev. Lett.* 70 (1993) 2399.
- [22] B.A. Malomed, A.A. Nepomnyashchy and A.E. Nuz, *Physica D* 70 (1994) 357.
- [23] G. D'Alessandro and W.J. Firth, *Phys. Rev. A* 46 (1992) 537.